INL/EXT-17-41870
Revision: 0

Status Report on Pressure Resistance Weld Development for FeCrAl Thin-Wall Cladding

Fuel Cycle Research & Development Advanced Fuels Campaign

Jian Gan, Emmanuel Perez
Idaho National Laboratory

Nathan Jerred
University Space Research Association

Prepared for
U.S. Department of Energy
Office of Nuclear Energy

April 2017
NTRD-FUEL-2017-000363

INL/EXT-17-41870
Revision 0

Status Report on Pressure Resistance Weld Development for FeCrAl Thin-Wall Cladding

Jian Gan, Emmanuel Perez — INL
Nathan Jerred — University Space Research Association

April 28, 2017

Idaho National Laboratory
Idaho Falls, Idaho 83415

http://www.inl.gov

Prepared for the
U.S. Department of Energy
Office of Nuclear Energy
Under DOE Idaho Operations Office
Contract DE-AC07-05ID14517

INTENTIONALLY BLANK

ABSTRACT

This report summarizes the recent development on the weld techniques of joining the thin-walled FeCrAl cladding to the endplug as a part of accident tolerant fuels (ATF) program for advanced light water reactor (LWR) systems. The FeCrAl alloy has been considered as the top candidate cladding materials for ATF fuels largely due to its high oxidation resistance in high temperature steam relevant to the loss of coolant accident (LOCA) conditions. The two primary techniques for the thin-walled cladding weld development are laser beam weld (fusion based) and pressure resistance weld (solid state without melting). This report focuses on the progress made on the pressure resistance weld (PRW) development for a commercial FeCrAl alloy.

INTENTIONALLY BLANK

CONTENTS

ABSTRACT v

1. INTRODUCTION 1

2. PRW DEVELOPMENT FOR FE-CR-AL THIN-WALL CLADDING 4

3. MICROSTRUCTURE CHARACTERIZATION OF PRW 21

4. MICROHARDNESS OF PRW BOND REGION 23

5. HYDRAULIC PRESSURE BURST TEST OF PRW 24

6. CONCLUSIONS 26

FIGURES

Figure 1. A customized PRW system with an electrical current pulse capacity up to 30,000 Amps in less than 100 ms and a pneumatic cylinder capable of applying up to 1200 lbs force. The red box marks the fixtures holding the cladding-endplug samples with details shown in the following figure. 2

Figure 2. PRW electrode adapter loaded with endplug on the moving stage (left) and the surrogate thin-wall cladding on the fixed stage (right) with a stick-out length as a variable for PRW process 2

Figure 3. Samples of PRW with emulated endplug (top-left), the thin-wall cladding (top-right) and the welded sample set after PRW joining (bottom) ready for tensile test. 3

Figure 4. Sample design for PRW for endplug (left) and a thin-wall cladding (right). The threads are for tensile testing of the endplug-cladding weldment. 3

Figure 5. Schematic of the surrogate endplug (1) and thin-wall cladding (3) for PRW. The adapter (2) is for hydraulic pressure burst testing of the endplug-cladding weldment 4

Figure 6. PRW bonding schedules-1 (top-left), schedule-2 (top-right) and schedule 3 (bottom) are used for FeCrAl samples. 6

Figure 7. Sample 29-1 joined using PRW schedule-3 revealed severe material loss through ablation with a hole formed on the cladding at the weld zone 6

Figure 8. Optical images of Kanthal-D FeCrAl sample Set #33 after PRW. 8

Figure 9. X-ray CT scan of cross sectional view of the weld zone in samples 33-1 through 33-6. 8

Figure 10. The plot of power as a function of time for the main heat process of the schedule-2for samples 33-1, 3, 4, 6 & 7. Note that the scale for power for bottom plot is doubled than the top plot. 9

Figure 11. X-ray CT cross sectional images of PRW bond region reveal the quality of the bond and the associated deformation on cladding and endplug for sample 33-8 through 33-13. 11

Figure 12. The plots of power as a function of time for (A) comparison for sample 33-4 and sample 33-6 through 33-11, (B) pre-heat and mainheat phase for sample 33-12 and 33-13, (C) mainheat phase for sample 33-11 and 33-12. 12

Figure 13. Stress-strain curves (left) for tensile test of PRW sample 33-10 through 33-13 after PWHT and the images (right) of samples after tensile test. 13

Figure 14. Images of sample 34-1 through 34-4 after PRW and PWHT where sample 34-1 was severely misaligned. 15

Figure 15. The plot of power vs. time for PRW joining of sample 34-1 through 34-4. 15

Figure 16. X-ray CT 3D tomography showing a virtual cross-section of PRW bonding zone for samples 34-2, 34-3 and 34-4. 15

Figure 17. Stress-strain curve (top) from tensile test of sample 34-2 and 34-4 and images (bottom) of the samples after tensile test. 16

Figure 18. Images of sample 35-1 through 35-5 after PRW and these samples will be used for tensile test of as-welded conditions without PWHT. 17

Figure 19. The profile of power vs. time for sample set 35 consistent to that of sample set 34. 17

Figure 20. X-ray CT images of cross sectional view of the PRW bond region for sample set 35. Note that samples 35-1 & 35-2 were analyzed via a North Star Imaging X-ray CT system, where samples 35-3, 35-4 & 35-5 were analyzed via an Adaptive Energy X-ray CT system 18

Figure 21. Stress-strain curve (top) from tensile test of sample 35-2 and 35-4 and images (bottom) of the samples after tensile test revealed significant deformation on the cladding and failure outside the weld zone. 19

Figure 22. Comparison of tensile test results between sample set 34 (with PWHT) and set 35 (without PWHT). 20

Figure 23. Images of sample Set 36 after PRW joining under the same conditions with sample set 35. 21

Figure 24. X-ray CT images of cross sectional view of the PRW bond region for sample set 36. 21

Figure 25. Optical microscopy of cross sectional view revealed the PRW bond region for sample 34-3. 22

Figure 26. EBSD orientation map of the PRW bond region revealed good metallurgical bonds at the joining interface between the thin-wall cladding and endplug for sample 34-3. 22

Figure 27. Optical microscopy image of microhardness indentation grid for PRW sample 34-3. 23

Figure 28. Hardness plot along the lines in the above figure revealed minor change in the bond region. 23

Figure 29. Images of the experimental setup for hydraulic pressure burst test at room temperature and high temperatures (left) and the details of the PRW bonded sample connected to the adapter (right). 24

Figure 30. PRW sample 36-1 through 36-4 after pressure burst tested at room temperature in PWHT condition revealed failure at bond region. 25

Figure 31. Pressurization profile for burst test at room temperature for sample 36-1 through 36-4. 25

Figure 32. Hardness map with test grid, bond line and the lines of indents for hardness plot for PRW sample 24-5 made from Kanthal-D FeCrAl alloy. 26

TABLES

Table 1. PRW test matrix for sample Set #33 with endplug stick-out of 2.54 mm and time cycles of 2. 7

Table 2. Tensile test results for PRW sample 33-10 through 33-13 after PWHT. 14

Table 3. PRW joining parameters for samples 34-1 through 34-4 with 2 cycles for mainheat and 2.54 mm stick-out for endplug 14

Table 4. Tensile test of PRW sample 34-2 and 34-4 in PWHT condition. 16

Table 5. PRW parameters for sample set 35 under the same condition for sample set 34 except no PWHT. 17

Table 6. Tensile test of PRW sample 35-2 and 34-5 in as-joined condition without PWHT. 19

Table 7. Hydraulic pressure burst test results for sample 36-1 through 36-4 in PWHT condition. 25

INTENTIONALLY BLANK

Status Report on Pressure Resistance Weld Development for FeCrAl Thin-Wall Cladding

1. INTRODUCTION

Development of accident tolerant LWR fuel requires the development of robust cladding materials with high strength at high temperatures, good corrosion resistance and radiation tolerance under normal operation, and excellent resistance to steam at very high temperature. One class of materials that has improved properties over the current LWR Zircaloy cladding under high temperature steam condition (T >1000°C) is a Fe-base stainless steel with higher Cr and Al additions (FeCrAl alloy). The Al (~5 wt.%) in FeCrAl alloy forms Al_2O_3 at the alloy surface which is much more protective than Cr_2O_3 in conventional stainless steel under high temperature steam condition. This alloy has been considered a top candidate for the LWR accident tolerant fuel (ATF) cladding material.

Five detailed summary reports were issued previously (INL/LTD-13-30804, 14-31551, 15-34684, 15-36583, 16-39760) on the weld development for thin-wall cladding made from MA 956 oxide dispersion strengthened (ODS) alloy (an ODS FeCrAl alloy), commercial FeCrAl alloy (Kanthal-D) and experimental FeCrAl alloys developed by Oak Ridge National Laboratory (ORNL). The development of weld techniques in this project was focused on laser beam welding (LBW) and pressure resistance welding (PRW). The former is a high energy intensity fusion-based weld while the latter is a solid-state weld without melting. PRW technique is important since it is currently used for LWR fuel fabrication. Once the process parameters are optimized, the PRW only takes approximately 20 ms for each joining, significantly faster and more efficient than that of laser beam weld. PRW is also the preferred technique if ODS FeCrAl alloy is used for thin-wall cladding for ATF fuels.

This report will focus on the recent work since the issuing of the last PRW summary report (INL/LTD-15-36583) on the PRW for ~350 μm wall-thickness cladding and an emulated endplug fabricated from a commercially available FeCrAl alloy (Kanthal-D, 0.5 inch diameter solid bar). The thin-wall cladding was machined from a solid rod using gun drilling. Several modifications and improvement were made to the PRW system to ensure good alignment and Ar gas coverage at the joining zone. The current PRW system lacks the fine control of (1) the position and rotation of the moving stage and (2) impact load at low load conditions because it was not designed to join the thin-wall cladding.

Nevertheless, with effort on optimization of the system setting and several modifications to the endplug design, a reasonably good metallurgical bonding was achieved as confirmed from grain texture imaging and orientation mapping from the electron back-scattering diffraction (EBSD). The recent tensile testing of the PRW welded endplug and thin-wall cladding set shows promising result. However, the preliminary hydraulic pressure burst test (HPBT) of the sample set joined using the same PRW conditions revealed that the failure occurred at hydraulic pressure significantly lower than that of laser beam weld. This indicates that further modification of the endplug design for PRW is necessary.

An overview of the PRW system is shown in Figure 1. Both the fixed and moving stage adapters are shown in Figure 2. A typical pair of surrogate thin-wall cladding and endplug is shown in Figure 3. Figure 4 shows the design details of the PRW sample set for endplug and thin-wall cladding. For the tensile testing of the weldment, primary endplug – cladding tube weld setup employs external threaded ends to pair with the tensile testing fixtures. For rupture testing of the weldment with HPBT, the endplug incorporates internal threads to accept a 1/16” MNPT fitting which pairs with the rupture testing equipment and the endplug has a 1/16” diameter through-hole to facilitate internal pressurization. A schematic of PRW sample set for HPBT is shown in Figure 5.

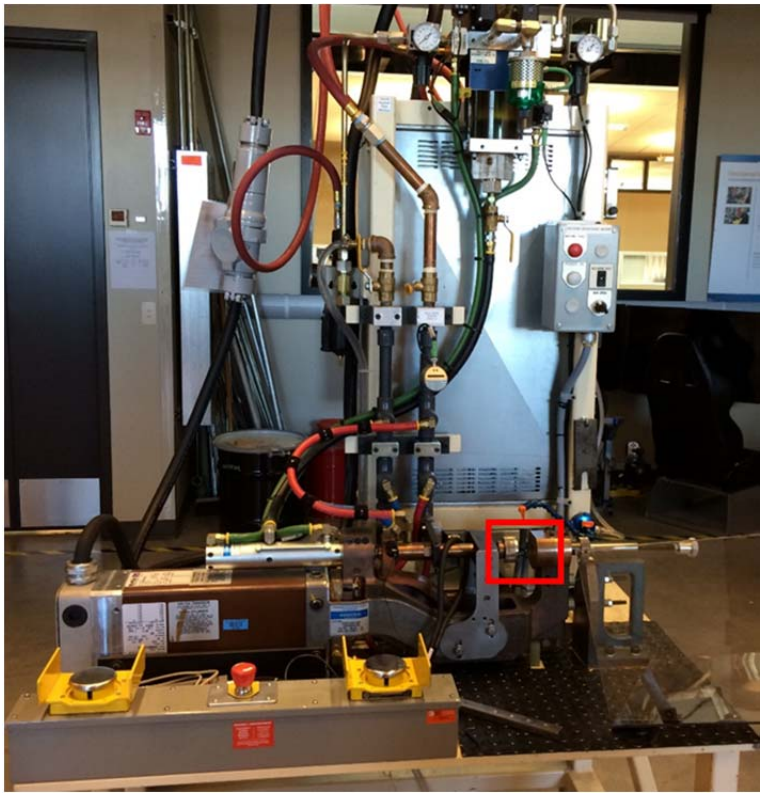

Figure 1. A customized PRW system with an electrical current pulse capacity up to 30,000 Amps in less than 100 ms and a pneumatic cylinder capable of applying up to 1200 lbs force. The red box marks the fixtures holding the cladding-endplug samples with details shown in the following figure.

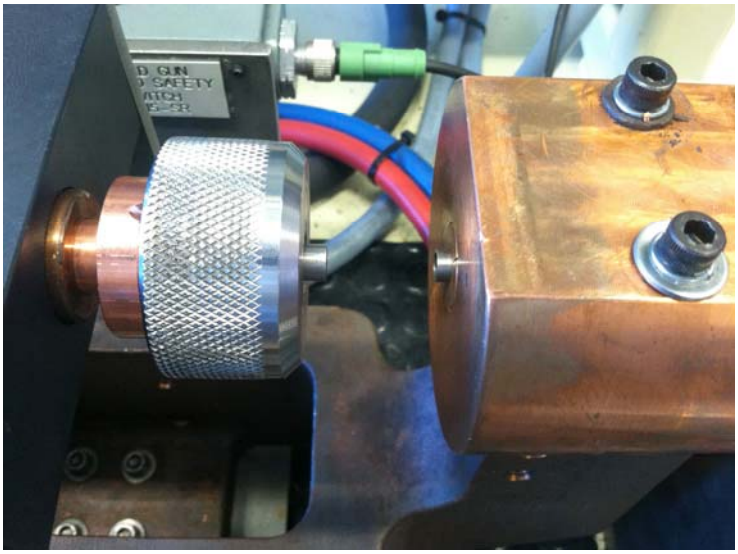

Figure 2. PRW electrode adapter loaded with endplug on the moving stage (left) and the surrogate thin-wall cladding on the fixed stage (right) with a stick-out length as a variable for PRW process.

Figure 3. Samples of PRW with emulated endplug (top-left), the thin-wall cladding (top-right) and the welded sample set after PRW joining (bottom) ready for tensile test.

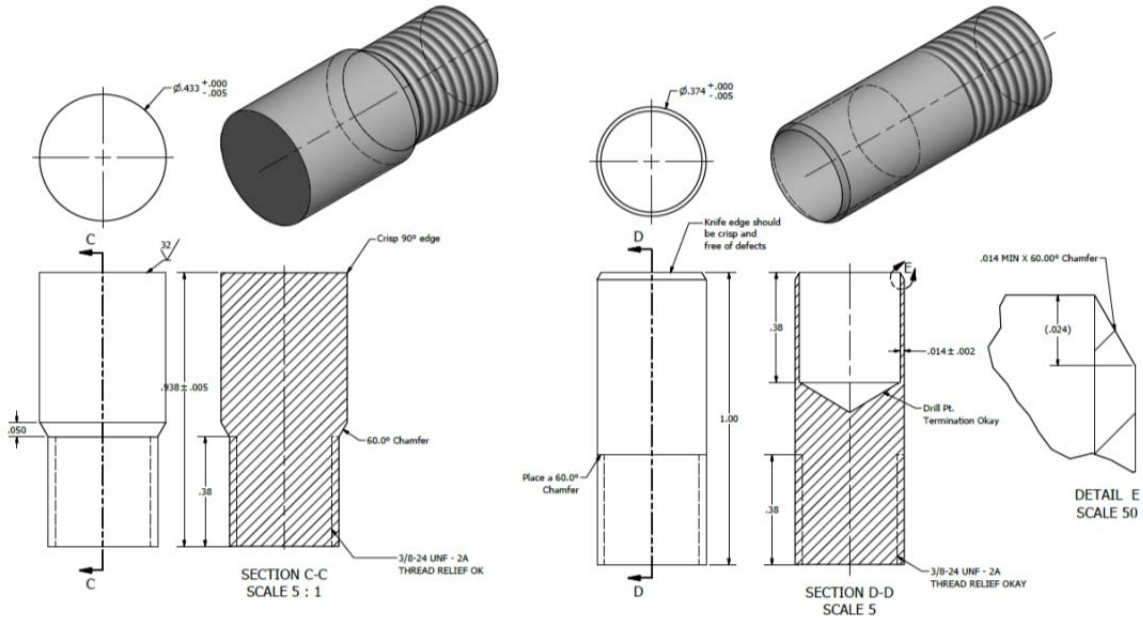

Figure 4. Sample design for PRW for endplug (left) and a thin-wall cladding (right). The threads are for tensile testing of the endplug-cladding weldment.

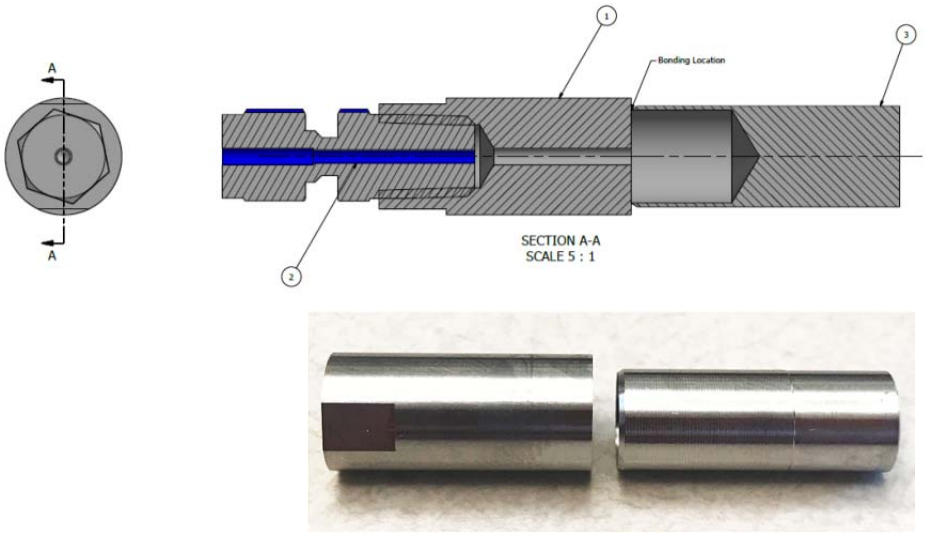

Figure 5. Schematic of the surrogate endplug (1) and thin-wall cladding (3) for PRW. The adapter (2) is for hydraulic pressure burst testing of the endplug-cladding weldment.

2. PRW DEVELOPMENT FOR FE-CR-AL THIN-WALL CLADDING

PRW is a localized thermal-mechanical joining process without melting. The primary heating mechanism for pressure resistance weld is based on Joule heating. Significant effort went into investigating the PRW using a customized system including modifications of endplug configuration to confine the heating zone and modifications of the PRW system to improve the alignment which is critical for joining the thin-walled cladding to endplug. It is very important to maintain a uniform, confined and good electrically conductive contact interface when passing very large electrical current to ensure a uniform heating at the joining interface. The electrode on the thin-wall cladding must be very close to the joining line (< 2 mm) to confine the heating zone in order to reduce the heat affected zone (HAZ) outside the weld zone. For PRW of FeCrAl material, an initial mechanical impact before passing the large current is necessary to break the surface oxide layer and ensure good electrical conduction at the faying interface.

The experimental work for PRW of thin-wall cladding includes sample fabrication, PRW joining, non-destructive imaging of the weldment including X-ray 3-D computed tomography (CT), post-weld heat-treatment (PWHT), microstructural analysis of the cross-sectioned sample, tensile testing, microhardness test and hydraulic pressure burst test. The endplug faying surface was mechanically polished down to 1200 grit SiC papers to minimize surface roughness. Prior to PRW joining, all weldments are thoroughly cleaned with ultrasonic bath in acetone followed by in ethanol. Electrode parts are wiped clean using ethanol. The electrical-based joining parameters were recorded onto a laptop computer through the joining process using a microcontroller that is paired with an inductance loop around the delivery electrode and alligator clamps placed on each electrode. Data is measured at a ½ cycle resolution, where 1 cycle = 16.67 ms. Data recorded includes time, resistance, current and voltage. Recorded data can be plotted and used to evaluate any anomalies experienced through a joining process and allows for consistency in the bonding process to be monitored. The data also allows for the total bonding energy deposited through the joining process to be calculated. Power is calculated by $P = I^2 \cdot R$

where I is the electrical current and R is the resistance. Total joining energy can be calculated by integrating the area under the power vs. time plot curve.

Bonded samples were analyzed through the non-destructive imaging technique, X-ray 3D CT scan to visualize weld quality. Two different x-ray setups were used: (1) A North Star micro focus x-ray system using a 130 kV Hammatsu x-ray source paired with a Varian detector, (2) An Adaptive Energy THX 1138 with a 225 kV x-ray source and a Varian detector. Both are capable to visualize the small cracks of a few µm in size. The PWHT process was carried out at 700 °C for 2 hours in a CM tube furnace utilizing a continual flow of ultra-high purity (UHP) argon gas followed by a furnace cool. Cross-Section Analysis of Samples includes optical microscopy (OM), scanning electron microscopy (SEM) and x-ray diffraction (XRD). Sample surfaces were prepared through normal sample preparation steps using both SiC polishing papers and diamond suspension on a vibratory polisher using 0.05µm colloidal silica as the final polishing medium. Optical Microscopy was performed using a Keyence VHX 1000 digital microscope. SEM was performed using a JEOL JSM-6610LV TFG paired with a TSL Hikari electron backscatter diffraction (EBSD) detector. The XRD was performed using a Rigaku SmartLab X-Ray Diffractometer.

Mechanical characterization was performed via tensile testing, rupture testing & micro-indentation. Tensile testing was done using an Instron 5967 electromechanical system with an Instron 10 kN load cell with an extension rate of 10 µm/min. Micro-Indentation testing was conducted using a LECO LM 247AT auto-tester using a Vickers micro-indenter paired to AMH 43-1.71 Software to analyze hardness data. The Indent load is 100 g force with a dwell time of 13 sec. Hydraulic pressure burst testing was carried out using an Additel 928 with a pressure range of 0 to 15000psi and a temperature range of RT to 180°C using mineral oil as the pressurizing fluid. The HPBT System uses a pressure transducer paired to a LabView suite to record data

For the PRW process three primary bonding schedules were employed, as shown in Figure 6, with small adjustments made to the electrical current and the stick-out length for the cladding between the various samples. Schedule-1 employs an impulse-based pre-heating phase followed by a continuous primary heating phase. There is a cooling cycle between each impulse heating – the use of small blast of current aims to disrupt the oxide layer and promote initial bonding. The pre-heat phase is followed by a quick slope increase to the primary heat phase which is held for several cycles. While the current is turned off the force is still maintained. This promotes a good metallurgical bond as well as a thermal cooling path between the water-cooled electrodes and the welded samples.

Schedule-2 is a simplified joining schedule that utilizes a single passage of current. It is identical to primary heat phase in Schedule-1 but without the pre-heat phase. In this study focus was on looking at the benefits of employing a pre-heat phase. Additionally, previous work indicated the use of a higher joining force resulted in better bonding characteristics, thus in this work a bonding force of 900 lbs (3996 N) was held constant. The PRW uses a two-step force process. The initial force is used to close the electrode gap and provide contact between the faying interfaces and then, once current is applied, the force is stepped up considerably and kept constant for the remaining joining process.

Schedule-3 was also evaluated that looked at limiting the amount of deformation that takes place through the joining process. The joining schedule is labeled ‘Reverse Load Profile’ where a high amount of force was applied prior to passing current, and when current was applied the joining force was stepped down to reduce the amount of deformation at the joining interface. Sample 29-1 was joined using Schedule-3 with a bonding force and a joining force of 900 lbs and 100 lbs, respectively. The resulting bond showed significant ablation loss of the tube material. The X-ray CT analysis showed the formation of a large hole in the cladding at the bond location as shown in Figure 7. No further joining was conducted under the schedule-3.

It was found that the joining force through the passing of electrical current must be greater than 100 lbs force to maintain the necessary contact pressure at the faying surfaces. Adequate contact pressure aids in driving down contact resistance which allows for more current to be applied to facilitating the bonding

between the endplug and cladding tube. The PRW process parameters for sample Set # 33 are listed in Table 1. Sample set 33 was primarily used for parameter optimization and to evaluate how changes in various variables affected the joining process and resulting bond. This sample set utilizes both schedule-1 and schedule-2, as previously discussed. Then parameters such as joining force, joining current, number of impulses, impulse current, tube stick-out length, etc. were all variables investigated. For this sample set the joining force varied between 250 lbs and 1100 lbs. The stick-out length for endplug is fixed at 2.54 mm. The time for primary heating is fixed at 34 ms (2 cycles). The results of these tests are summarized in the table. The optical images and the x-ray CT scan of the non-destructive cross sectional view of the weld zone for sample Set #33 after PRW are shown in Figure 8 and Figure 9, respectively.

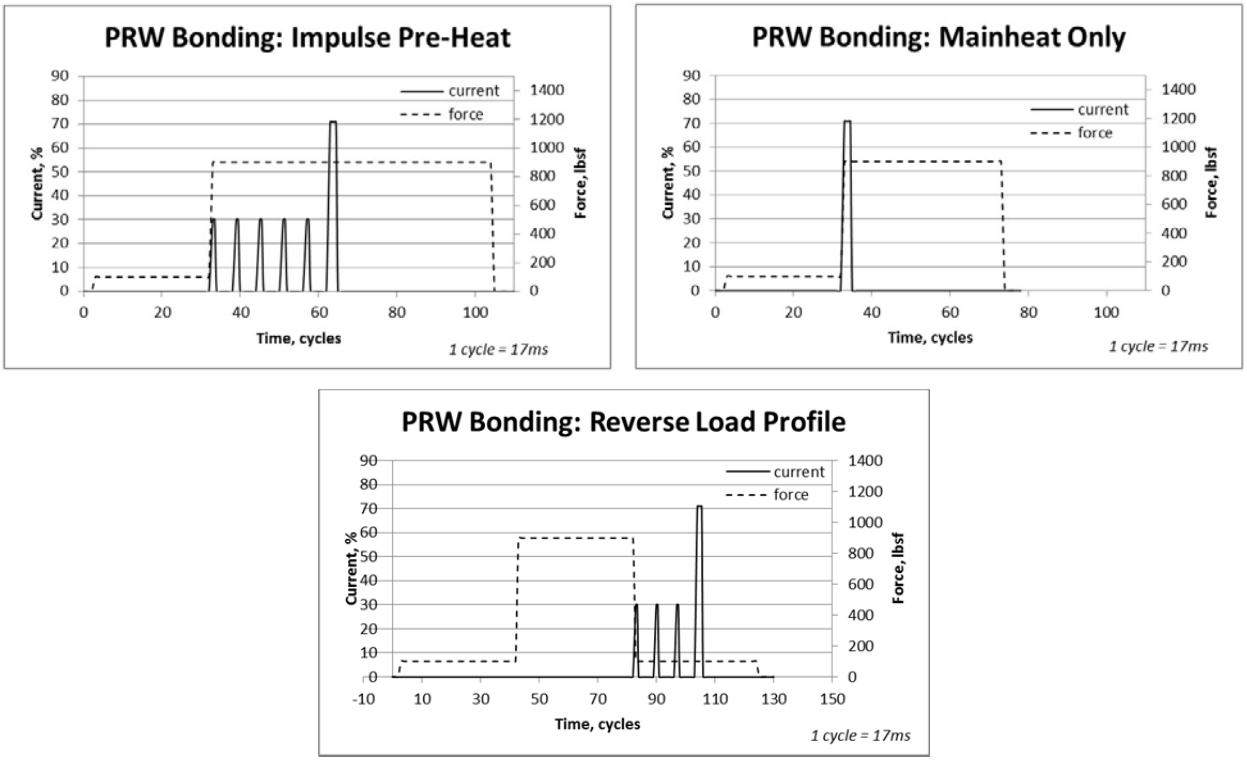

Figure 6. PRW bonding schedules-1 (top-left), schedule-2 (top-right) and schedule 3 (bottom) are used for FeCrAl samples.

Figure 7. Sample 29-1 joined using PRW schedule-3 revealed severe material loss through ablation with a hole formed on the cladding at the weld zone.

Table 1. PRW test matrix for sample Set #33 with endplug stick-out of 2.54 mm and time cycles of 2.

ID	Sch# \ Prg#	Appl. Force (lbs)	Clad Stick-out (mm)	Pre-heat current (%)	# of imp	Time (cycles) heat\cool	Primary Current (%)	Average mainheat current (kA)	Mainheat Joining Energy (J)	Comments
33-1	2\32	900	2.54	30	3	1\5	71	13.25	1162	Repeat sample 26-3, deformation occurred near end of pre-heat phase.
33-2	2\22	250	2.54	25	5	1\5	55	5.4	> 477[a]	Repeat 23-7, high heat seen through mainheat phase.
33-3	2\32	500	2.54	30	3	1\5	71	10.97	980	Repeat 33-1. Drop in force leads to low quality bond.
33-4[b]	1\40	1100	1.27	n/a	n/a	n/a	47	7.83	520	Higher joining force with smaller cladding stick-out. Bond looks good
33-5	2\41	250	2.54	25	3	1\5	55	5.36	807	Repeat 33-2 with reduced impulse. Sparks seen through mainheat phase.
33-6[b]	1\42	1100	1.27	n/a	n/a	n/a	94[d]	16.1	1877	Repeat 33-4 with increased current. Hole formed at bond region.
33-7	1\40	1100	1.27	n/a	n/a	n/a	40[e]	8.86	607	Follow-on from 33-6. No bond occurred although tube deformation occurred.
33-8[f]	1\43	1100	1.27	n/a	n/a	n/a	55	9.40	674	Follow-on from 33-7. No major expulsion seen at bond.
33-9	1\44	1100	1.27	n/a	n/a	n/a	61	11.04	859	Follow-on from 33-8. No sparks through joining. Some expulsion seen at bond.
33-10	1\45	1100	1.27	n/a	n/a	n/a	66	12.51	1005	Follow-on from 33-9. Achieved desired current of 12.4 kA. Good bond and expulsion formed at bond
33-11	1\46	1100	1.27	n/a	n/a	n/a	71	13.63	1147	Follow-on from 33-10 to increase current beyond 12.4 kA. Few sparks seen during joining.
33-12	2\32	1100	1.91	30	3	1\5	71	13.85	1181	Repeat 26-3 but changed to higher force 1100 lbs. Bonded w/o sparks
33-13	2\32	900	1.91	30	3	1\5	71	13.77	1179	Repeat 26-3 for tensile test comparison with 33-12.

a-data failed to record for several time-steps during joining making the calculated joining energy to be sufficiently low

b-An evaluation of previous resistance joining used for EBR-II fuel pin fabrication showed favorability using higher joining forces, thus joining force was increased to 1100 lbs force and based on current used to successfully join EBR-II fuel pins a target current of 12.4 kA was set for this work. In programming the joining current the inputs in the unit of amps were used.

c-Schedule programmed to deliver 12,000 amps however based on contact conditions at faying interface only 7,830 amps were achieved

d-Schedule programmed to deliver 15,000 amps however based on contact conditions at the faying interface 16,070 amps were achieved.

e-Schedule programmed to deliver 12,400 amps however based on contact conditions at the faying interface 8,860 amps were achieved.

f- A change was made in how electrical current is programmed in the joining process, instead of trying to achieve a known amperage by using the following input in amps- the joining process was changed back to programming a percent current, i.e. XX%I

Figure 8. Optical images of Kanthal-D FeCrAl sample Set #33 after PRW. Note that no bond occurred for sample 33-7.

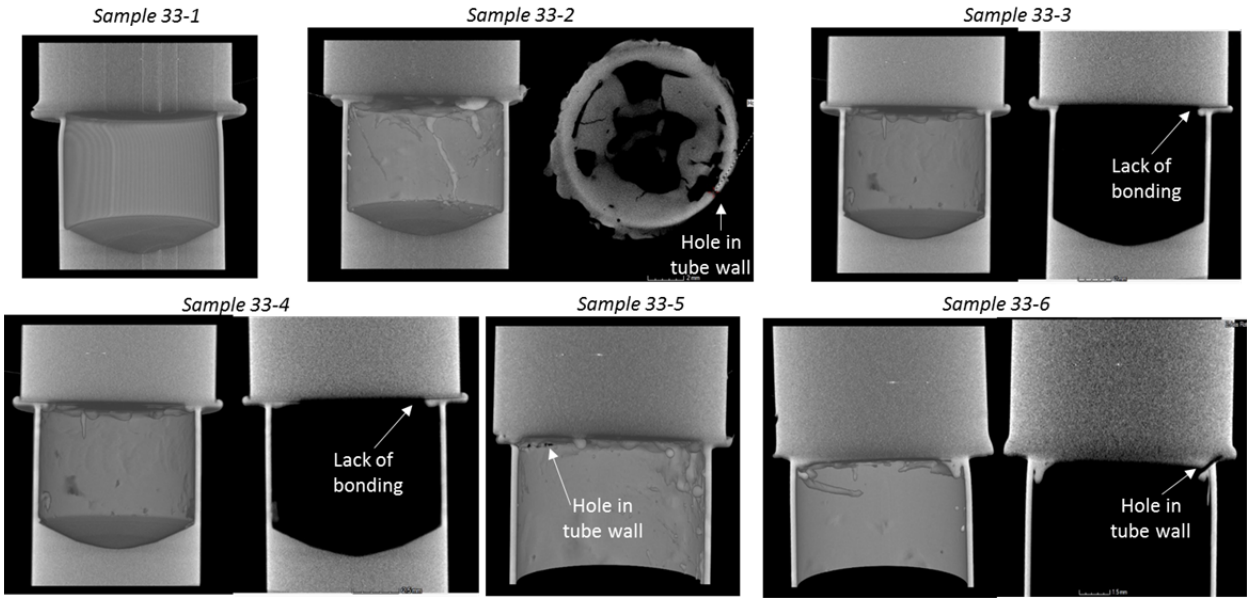

Figure 9. X-ray CT scan of cross sectional view of the weld zone in samples 33-1 through 33-6.

The power as a function of time for the main heat phase in schedule-2 process for samples 33-1, 3, 4, 6 & 7 is shown in Figure 10. Note there is a factor of 2 difference on the power scale between the two plots. It shows that energy deposition through the joining process in PRW can vary significantly depending on the process control setting and the condition at the contact interfaces between the endplug and thin-wall cladding. As a result of variable contact interface condition, it is not practical to control the exact power profile during the joining process with the current PRW system available for this project.

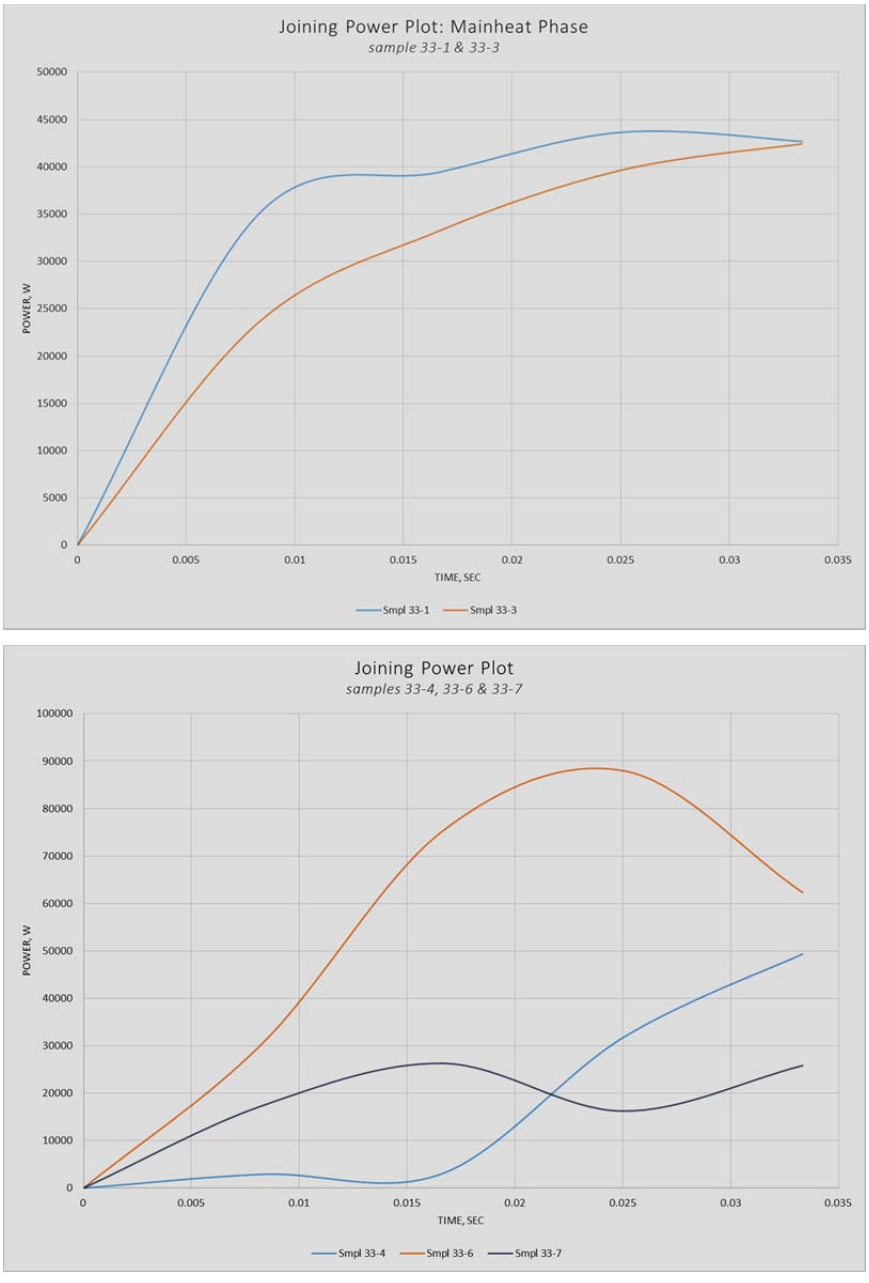

Figure 10. The plot of power vs. time for the main heat process of the schedule-2 for samples 33-1, 3, 4, 6 & 7. Note that the scale for power for the bottom plot is doubled compared to that of the top plot.

Samples 33-1 & 33-3 were joined using similar parameters and joining schedule where only the joining force was varied. Sample 33-1 showed significant deformation at the bond however the visual inspection showed no forging of the tube material into the endplug. Sample 33-3 was performed to decrease the deformation within the bond by lowering the applied force from 900 lbs to 500 lbs, but deformation in the cladding tube persisted and no deformation is seen in the endplug, i.e. lack of forging occurred, leading to limited bonding at several locations in the bond region. The power plot of the two samples shows that more power was developed through the joining process under the heavier load for sample 33-1.

Samples 33-2 & 33-5 were joined using similar parameters where the number of impulses was varied. Sample 33-2 showed excessive spallation, seen in CT images on the interior of the tube, and led to the formation of a hole in the tube wall. Sample 33-5 was performed to decrease the thermal input at the bond compared to sample 33-2 to limit or alleviate spallation of the tube material. This was done by decreasing the number of impulses in the preheating phase from 5 to 3 impulses. Even at the decreased number of preheat impulses, sample 33-5 still showed spallation of the tube leading to holes forming within the tube wall.

Samples 33-4, 33-6 & 33-7 were joined using similar parameters where the programmed current was varied. Based on the previous work on Experimental Breed Reactor-II (EBR-II) fuel pin fabrication, where pressure resistance welding was utilized with satisfactory results using a higher joining force, a joining current of 12.4kA and force of 1100 lbs was selected as a good starting point. Sample 33-4 used a joining force of 1100 lbs and was the first attempt to reach 12.4kA. However, the actual current achieved was significantly lower than the targeted current, leading to a poor bond. The difficulty in reaching the programmed current was believed to be due to contact effects at the faying interface. For sample 33-6 the current setting on the program was increased to accommodate contact effects, however, this time the current achieved far exceeded the targeted current, leading the excessive deformation and the formation of a hole within the bond region. The high current achieved for sample 33-6 shows contact effects may not hinder the current delivered through the joining process. For sample 33-7 the current setting was re-adjusted to 12,400 amps, however, as with sample 33-4 the current achieved was significantly lower leading to a sample that failed to achieve a bond. The variations in the power developed through the joining process can be seen in the power plots in Figure 10.

The X-ray CT cross sectional images of sample 33-8 through 33-13 reveal the extent of deformation in the bond, the expulsion formation and the quality of bond as shown in Figure 11. No major spallation was seen in these samples. Other visual indicators are the visualization of the bond line, the flatness of the bond line, deformation of the endplug and mixing/forging of the tube into the endplug. The plots of power as a function of time for sample 33-4 through 33-13 are shown in Figure 12 for comparison.

Samples 33-8, 33-9, 33-10 & 33-11 were all joined using similar parameters where the current setting was varied in an attempt to reach the target current of 12.4 kA. These samples were a continuation from samples 33-4, 33-6 & 33-7, however, for samples 33-8 through 33-11 the programming of current was performed using the input in percentage (%) instead of using the input in “Amps”, which was previously used for samples 33-4, 33-6 & 33-7. It is believed that the current in % is a more appropriate control parameter to get persistent current delivered through the joining process from sample to sample.

Samples 33-8, 33-9, 33-10 & 33-11 were joined using a current setting of 55%, 61%, 66% & 71%, respectively. Samples 33-8 & 33-9 showed bonding but CT imaging showed limited deformation in the bonding region and the bond line was still discernable. The joining of sample 33-10 achieved 12.5 kA, meeting the goal of 12.4 kA and sample 33-11 achieved 13.6 kA to evaluate the bond quality beyond 12.4 kA. CT imaging showed more deformation in the bond and better expulsion formation. The bond line appears less visible for samples 33-10 & 33-11. In evaluating the power plots for these samples they all trend a similar path with their respective delivered power steps up with increasing current.

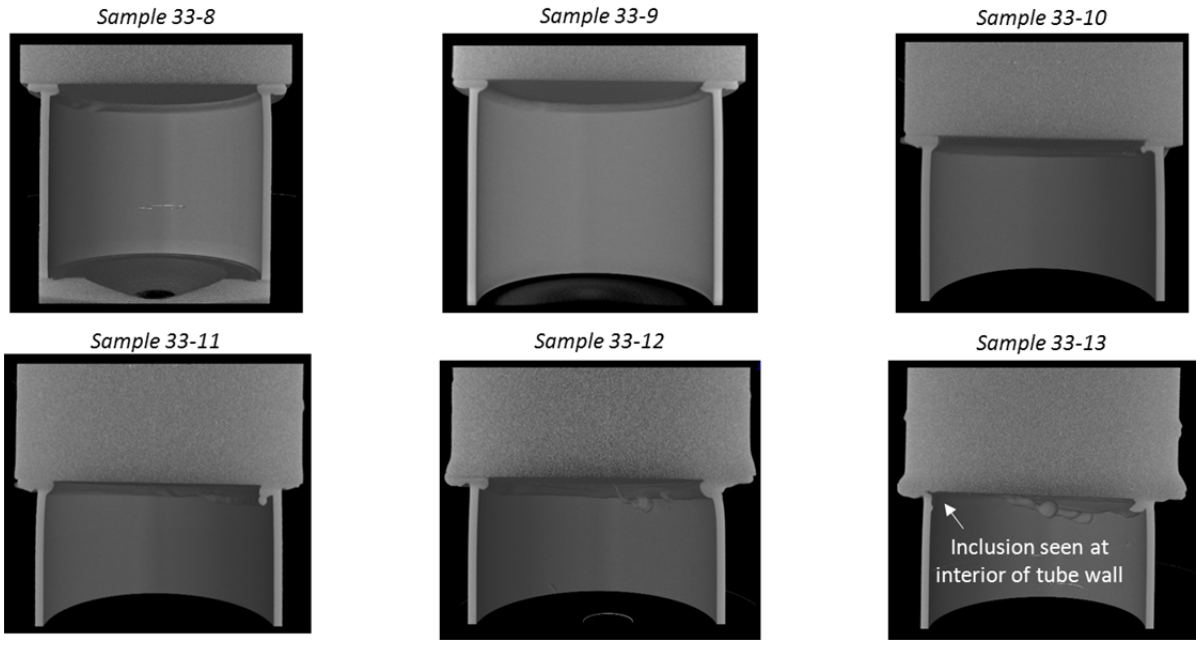

Figure 11. X-ray CT cross sectional images of PRW bond region reveal the quality of the bond and the associated deformation on cladding and endplug for sample 33-8 through 33-13.

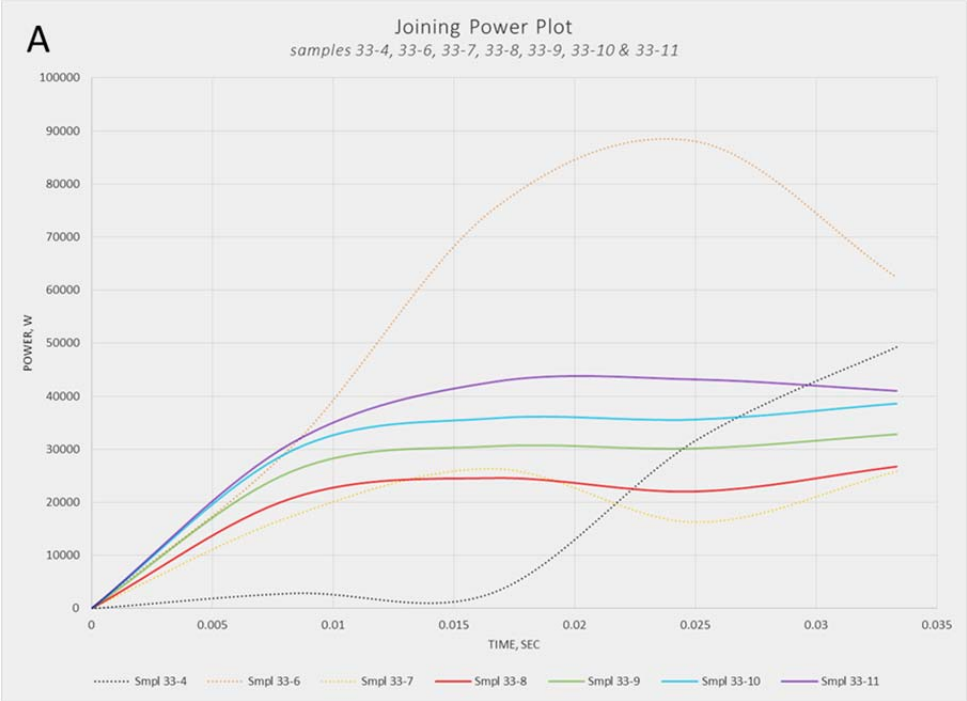

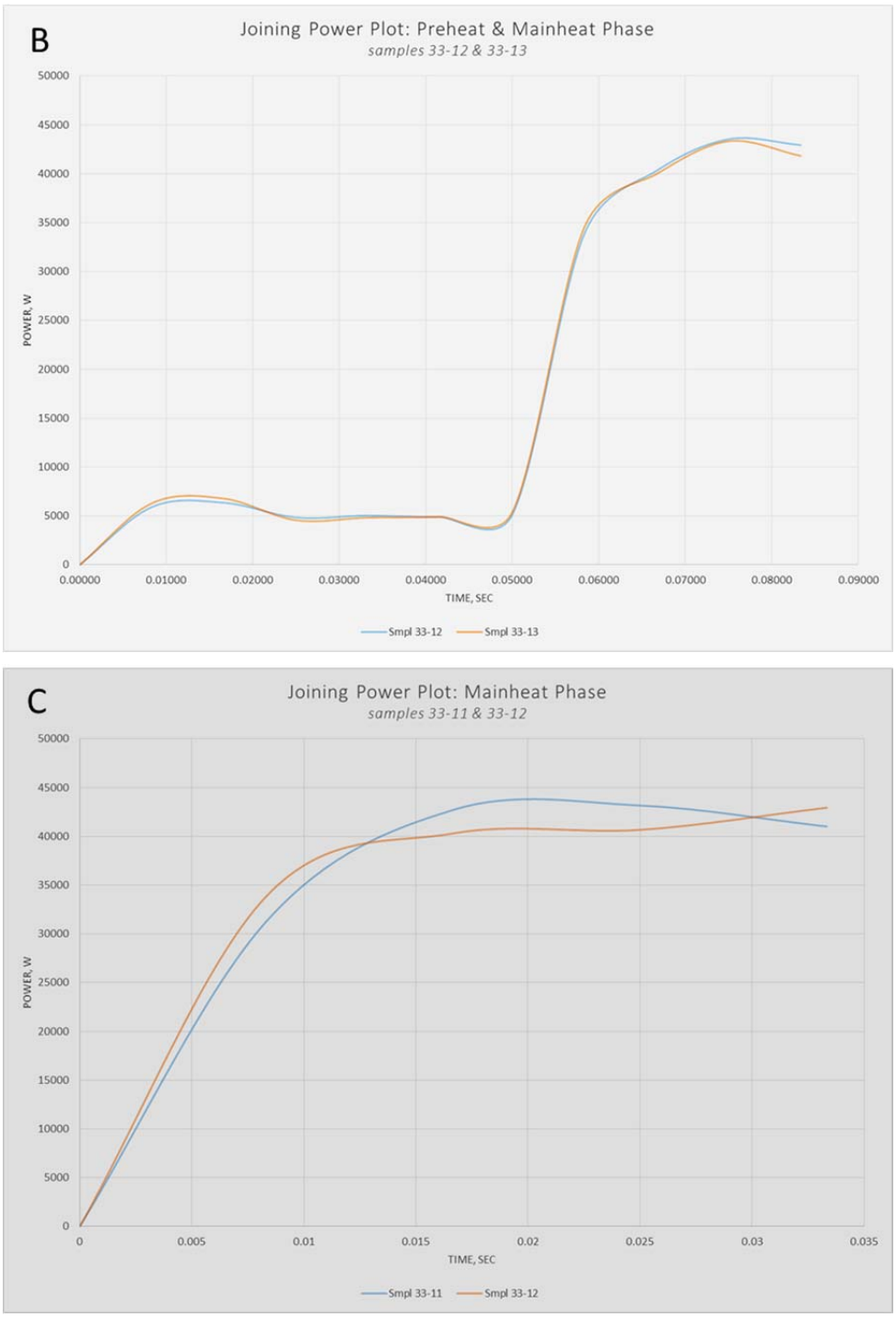

Figure 12. The plots of power as a function of time for (A) comparison for sample 33-4 and sample 33-6 through 33-11, (B) pre-heat and mainheat phase for sample 33-12 and 33-13, (C) mainheat phase for sample 33-11 and 33-12.

Sample 33-12 utilizes a joining schedule with an impulse-based preheat phase (joining schedule #2) and is a repeat of sample 26-3, which showed positive bond formation, but with an increase in joining force from 900 lbs to 1100 lbs. The bond formation via X-ray CT imaging looks good showing good deformation in the bond region and some expulsion formation. Additionally, the bond line is barely visible. The comparison between samples 33-11 and 33-12 shows the differences experienced between the two joining schedules, i.e. how an impulse pre-heat phase affects the overall bond formation. CT imaging shows much more deformation occurs in sample 33-12, especially apparent in the endplug. The plot of just the mainheat phase of these two samples shows that they trend together, indicating the preheat phase does not drastically affect the power-time profile of the mainheat phase.

Sample 33-13 is an exact repeat of sample 26-3 utilizing a joining force of 900 lbs. Therefore, when the bond is directly compared to that of sample 33-12 the variation in high joining forces can be evaluated. CT imaging shows good deformation in the bonding region however the cladding tube appears to have formed a slightly under-cut region in the tube wall. The plot of both samples shows a nearly identical power plot indicating a difference in applied bonding force between 1100 lbs to 900 lbs has little or no effect on the electrical characteristic of the weld zone during joining process, but such a change may affect the mechanics of the joining process such as amount of deformation. Based on the bond quality seen in CT imaging of sample 33-10 through 33-13, they will be subjected to follow-on tensile testing to mechanically test the PRW bond.

Before tensile testing, a post-weld heat treatment (PWHT) was applied to sample 33-8 through 33-13. It was performed at 700 °C for 2 hours in flowing ultrahigh purity argon gas at a flow rate of approximately 20 standard cubic feet per hour (SCFH), followed by cooling within the furnace. Samples 33-10 through 33-13 were tensile tested and the results and test conditions are shown in Figure 13 and Table 2. Note that the nominal tensile property for Kanthal-D FeCrAl alloy for yield stress and tensile strength is 470 MPa and 630 MPa, respectively. The yield stress for sample 33-10, 33-12 and 33-13 could not be determined since they all failed before reaching the yield point. Sample 33-11 revealed excellent mechanical properties of the weld with both yield stress and tensile strength exceeded the nominal values.

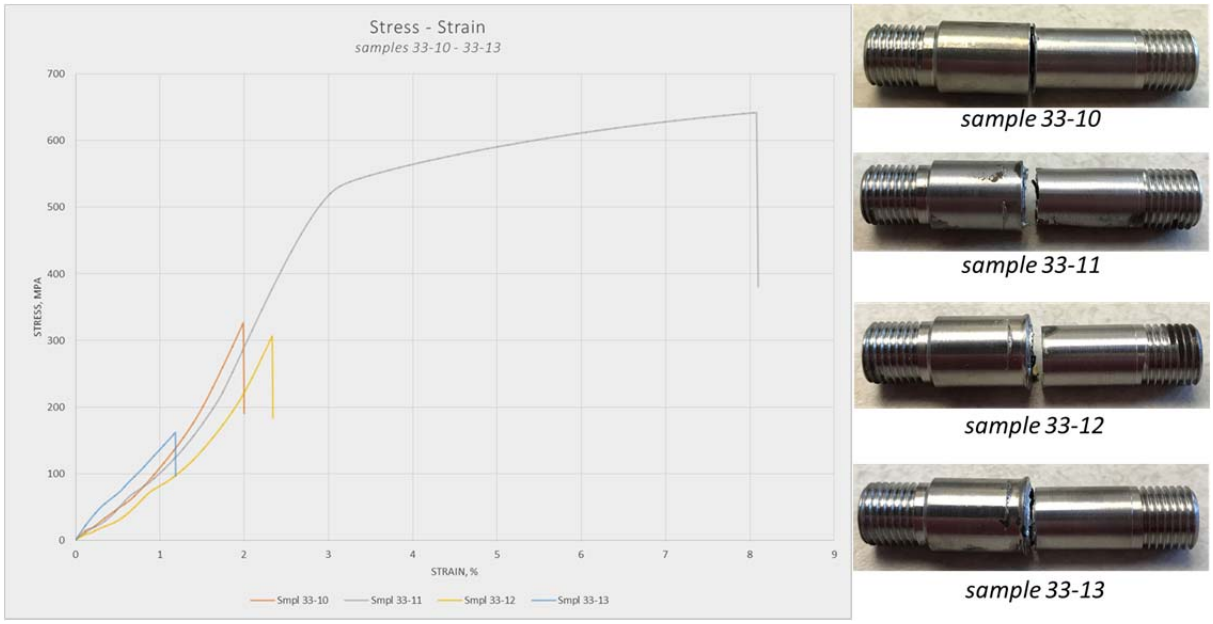

Figure 13. Stress-strain curves (left) for tensile test of PRW sample 33-10 through 33-13 after PWHT and the images (right) of samples after tensile testing.

Table 2. Tensile test results for PRW sample 33-10 through 33-13 after PWHT.

ID	Area (mm^2)	Max load (kN)	Max elongation (mm)	Max stress (MPa)	Max strain (%)	Yield stress (MPa)	Failure location
33-10	9.92	3.24	0.19	326	2.0	n/a	At bonding interface
33-11	10.00	6.41	0.77	642	8.1	527	Tube side near bond
33-12	10.10	3.10	0.22	307	2.3	n/a	Tube side near bond
33-13	9.96	1.61	0.11	162	1.2	n/a	Tube side near bond

Samples 33-10, 33-12 & 33-13 all failed within the elastic region of the stress-strain curve, where sample 33-11 showed plastic deformation prior to failure. Sample 33-10 failed at the bonding interface with the bond 'peeling' apart. Sample 33-11 showed favorable tensile results with failure occurring on the tube-side of the bond. Similarly, samples 33-12 & 33-13 both failed at relatively similar locations, just on the tube-side of the bond. CT imaging of sample 33-13 showed the tube had an undercut region in the tube, failure appears to have occurred at or near that location. In comparing samples 33-11 & 33-12, although the preheat phase of 33-12 promotes more deformation within the bonding region (see CT images) the preheat phase does not promote the formation of a bond with improved strength.

Based on the favorable tensile results seen in sample 33-11 all of sample set 34 specimens were joined using the same joining conditions. Sample set 34 specimens will be utilized for tensile testing to get more mechanical property data to correlate with samples 33-11 results. The PRW joining parameters for sample set 34 are listed in Table 3. The images of sample set 34 after PRW are shown in Figure 14 where sample 34-1 was severely misaligned. The plots of power as a function of time during PRW joining are shown in Figure 15. The power profiles for each weldment under the same condition are quite consistent. The deviation of the power profile for sample 34-1 is likely due to the severe misalignment.

Figure 16 shows the X-ray CT images of the cross sectional view of the bond region after PRW process for sample 34-2, 34-3 and 34-4. All three samples show similar bond formation. Good expulsion formed and the bond line is not visible. The cladding tube appears forged into the endplug which indicates a good bond. It can be seen that the bond deformation is not consistent around the entire bond. This may be due to how electrical current is passed through the weldments or due to the tube making contact with the endplug slightly to one side and inducing more deformation. Samples 34-2 & 34-4 were passed on for tensile testing and sample 34-3 was cross-sectioned for microstructural characterization.

Table 3. PRW joining parameters for samples 34-1 through 34-4 with 2 cycles for mainheat and 2.54 mm stick-out for endplug.

ID	Sch# \ Prg#	Appl. Force (lbs)	Clad Stick-out (mm)	Pre-heat current (%)	# of imp	Time (cycles) heat\cool	Primary Current (%)	Average mainheat current (kA)	Mainheat Joining Energy (J)	Comments
34-1	1\46	1100	1.27	n/a	n/a	n/a	71	13.17	1164	Sample misaligned
34-2	1\46	1100	1.27	n/a	n/a	n/a	71	12.54	1135	Good weld formed
34-3	1\46	1100	1.27	n/a	n/a	n/a	71	13.05	1128	Good weld. Some slag seen on endplug past joining
34-4	1\46	1100	1.27	n/a	n/a	n/a	71	13.13	1134	Good weld formed

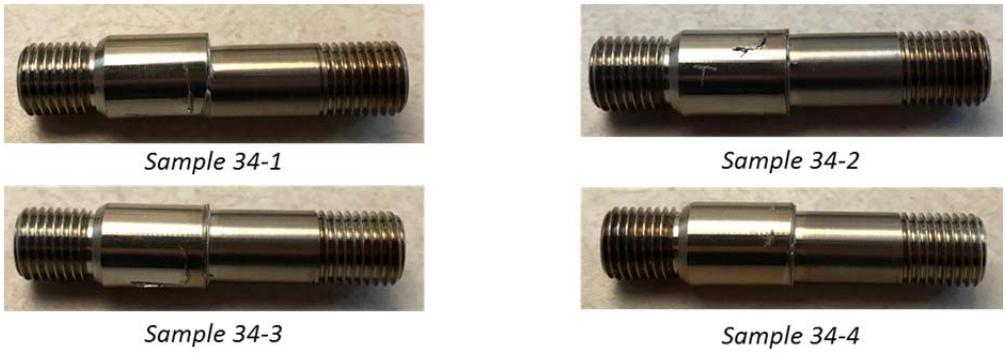

Figure 14. Images of sample 34-1 through 34-4 after PRW and PWHT where sample 34-1 was severely misaligned.

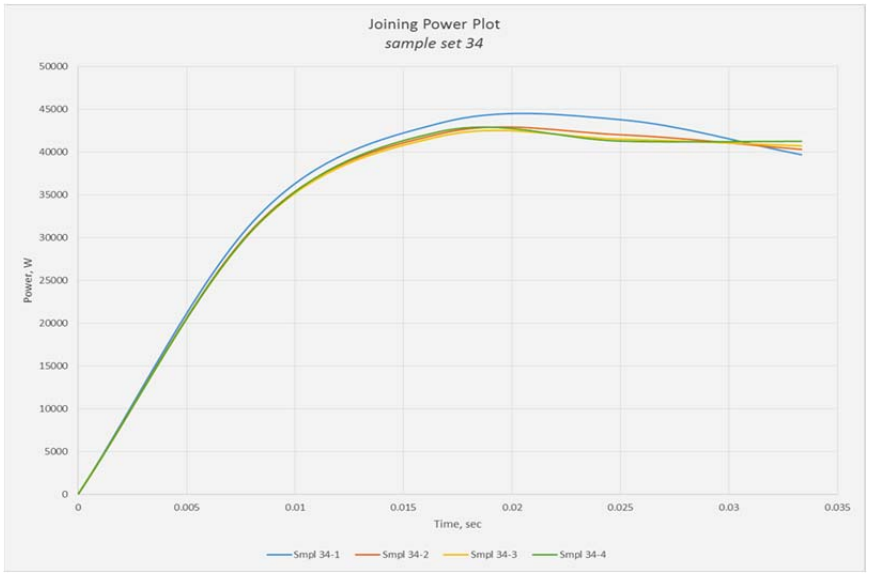

Figure 15. The plot of power vs. time for PRW joining of sample 34-1 through 34-4.

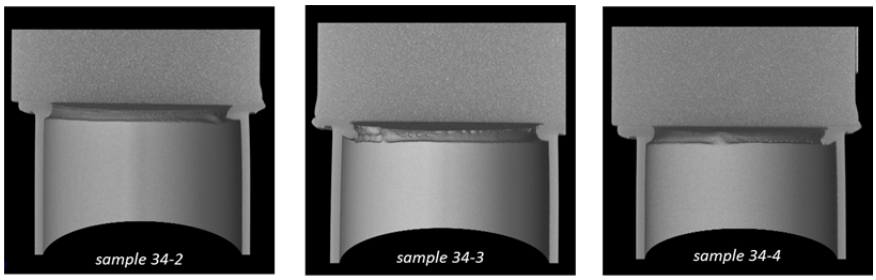

Figure 16. X-ray CT 3D tomography showing a virtual cross-section of PRW bonding zone for samples 34-2, 34-3 and 34-4.

The stress-strain curves of the tensile tests for samples 34-2 and 34-4 and the images of the samples after tensile test are shown in Figure 17 along with that of sample 33-11 for comparison under the same PRW condition. The tensile test conditions and results are summarized in Table 4. Samples 34-2 & 34-4 both showed tensile strength exceeding the materials yield strength prior to failure. Visually, both samples shows elongation of the tube section (pics on previous slide), where sample 34-2 exhibited more tube elongation prior to failure. Sample 34-2 showed failure at the bonding interface with the bond 'peeling' apart, where sample 34-4 showed failure in the tube next the bonding region. Additionally, sample 33-11 tensile data is plotted along with sample 34-2 & 34-4 showing all three samples show generally similar tensile performance.

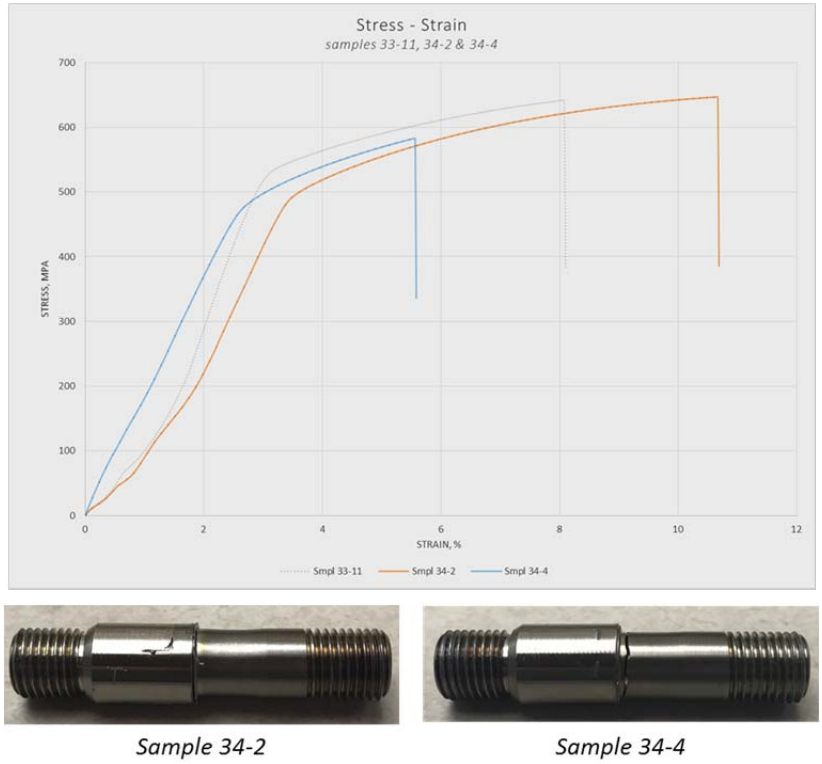

Figure 17. Stress-strain curve (top) from tensile test of sample 34-2 and 34-4 and images (bottom) of the samples after tensile test.

Table 4. Tensile test of PRW sample 34-2 and 34-4 in PWHT condition.

ID	Area (mm^2)	Max load (kN)	Max elongation (mm)	Max stress (MPa)	Max strain (%)	Yield stress (MPa)	Failure location
34-2	10.39	6.73	1.02	647	10.7	500	At the bonding interface
34-4	10.42	6.07	0.53	583	5.6	484	Tube side of the bond region

Sample set 35 specimens were joined using the same joining parameters used for sample set 34. However, sample set 35 did not undergo a PWHT process in order to characterize the bonding region and to evaluate the bonding strength of specimens in the 'as-joined' conditions. The PRW parameters, images of the samples after PRW and the plots of power vs. time during joining are shown in Table 5, Figure 18 and Figure 19, respectively.

Table 5. PRW parameters for sample set 35 under the same condition for sample set 34 except no PWHT.

ID	Sch# \ Prg#	Appl. Force (lbs)	Clad Stick-out (mm)	Pre-heat current (%)	# of imp	Time (cycles) heat\cool	Primary Current (%)	Average mainheat current (kA)	Mainheat Joining Energy (J)	Comments
35-1	1\46	1100	1.27	n/a	n/a	n/a	71	11.73	1135	Good bond although current slightly low.
35-2	1\46	1100	1.27	n/a	n/a	n/a	71	13.22	1158	Good bond
35-3	1\46	1100	1.27	n/a	n/a	n/a	71	12.47	1162	Good bond. Tube appears slightly skewed in top/bottom direction
35-4	1\46	1100	1.27	n/a	n/a	n/a	71	13.15	1153	Good bond
35-5	1\46	1100	1.27	n/a	n/a	n/a	71	13.25	1167	Good bond. Tube appears slightly skewed in side-side direction

Figure 18. Images of sample 35-1 through 35-5 after PRW and these samples will be used for tensile test of as-welded conditions without PWHT.

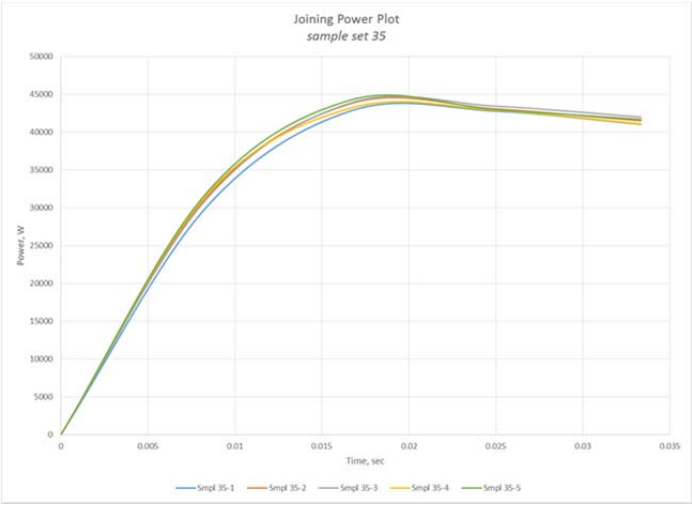

Figure 19. The profile of power vs. time for sample set 35 consistent to that of sample set 34.

Samples 35-1 & 35-2 were analyzed via a North Star Imaging Xray CT system, where samples 35-3, 35-4 & 35-5 were analyzed via an Adaptive Energy Xray CT system. In general all the samples show good deformation but the bond formation is not the same between all five samples. Sample 35-1 experienced less current during joining which may attribute to its difference in bond formation and limited endplug deformation. Samples 35-2 & 35-4 show good deformation between the endplug and cladding. The bond line is not easily visualized in either and the bonding region is slightly angled – especially in sample 35-2. The skewed alignment of sample 35-3 & 35-5 can be seen in the CT imaging. For sample 35-3 it is less obvious. For sample 35-5, the misalignment is much more obvious leading to a poor bond formation and the bond line can be discerned within the bonding region. Samples 35-2 & 35-4 were subjected to tensile testing. Sample 35-3 was utilized for microstructural characterization, targeting a cross-section plane 90° offset from the skewed direction.

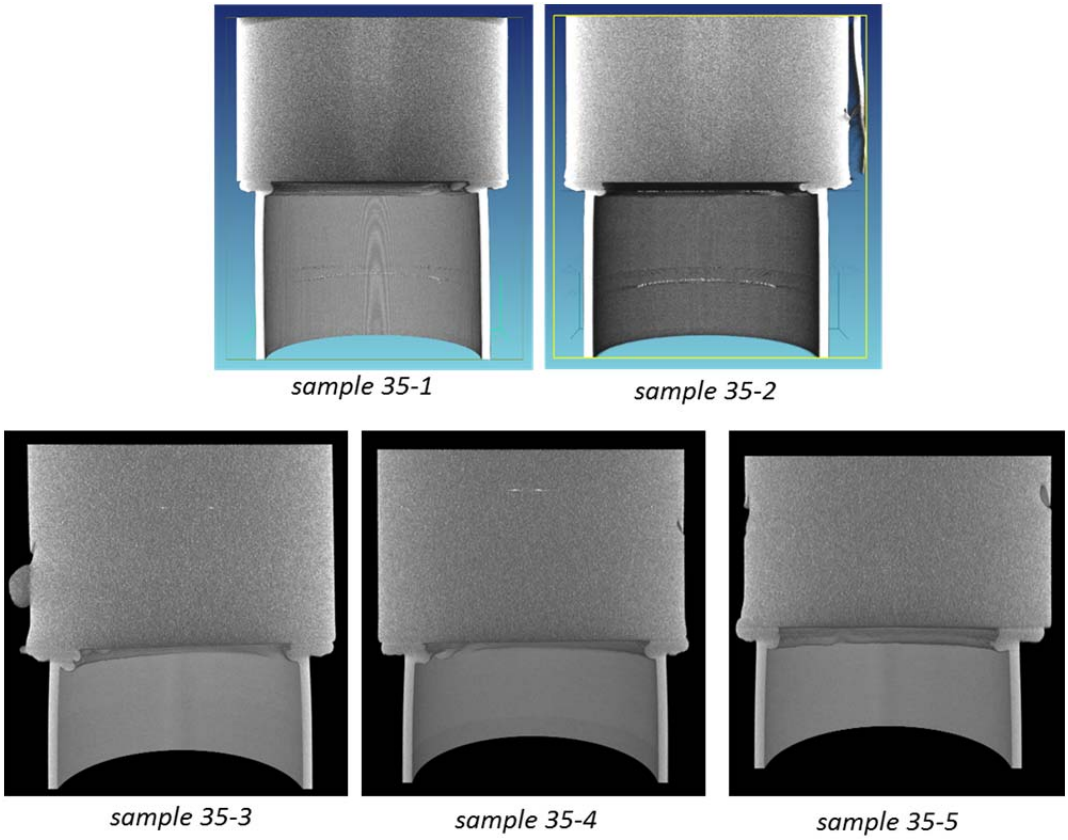

Figure 20. X-ray CT images of cross sectional view of the PRW bond region for sample set 35. Note that samples 35-1 & 35-2 were analyzed via a North Star Imaging X-ray CT system, where samples 35-3, 35-4 & 35-5 were analyzed via an Adaptive Energy X-ray CT system .

Samples 35-2 & 35-4 were tensile tested in the ‘as-joined’ condition without PWHT and both samples showed extensive deformation in the tube material (see pictures in previous slide) prior to failure, shown in Figure 21 and summarized in Table 6. Additionally, the samples experienced complete failure within the tube section showing the bond strength exceeds that of the tensile strength of the material. Also, it should be noted the yield strength and tensile strength reported for each sample tested agrees with the values reported for Kanthal-D material.

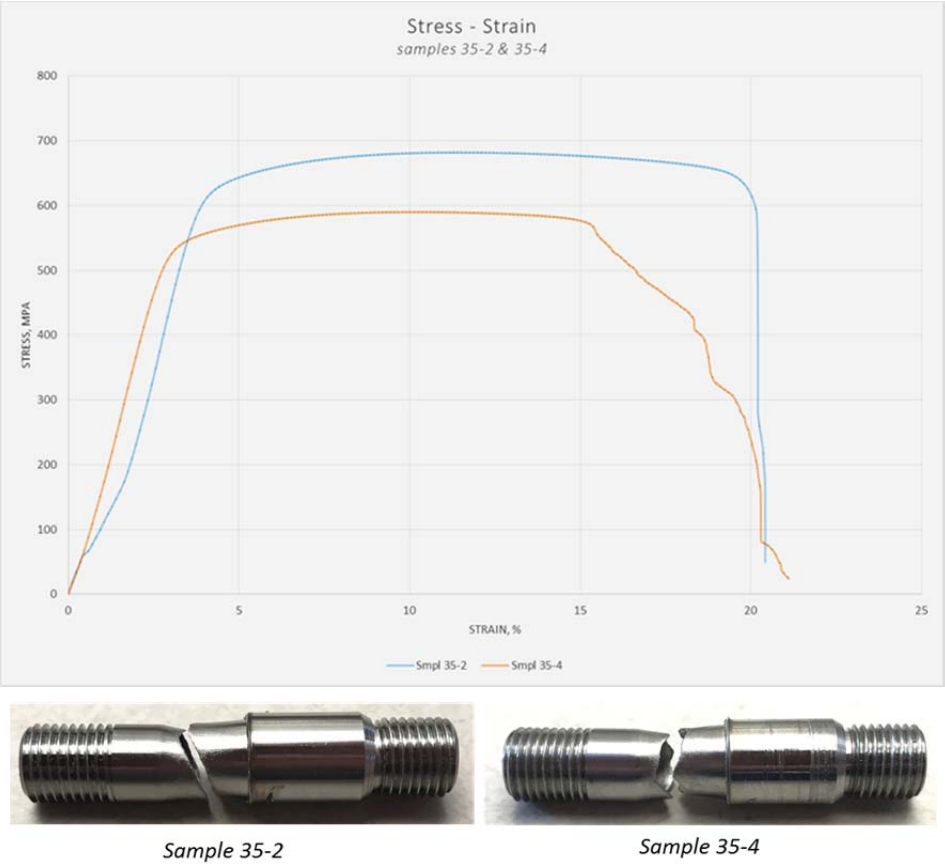

Figure 21. Stress-strain curve (top) from tensile test of sample 35-2 and 35-4 and images (bottom) of the samples after tensile test revealed significant deformation on the cladding and failure outside the weld zone.

Table 6. Tensile test of PRW sample 35-2 and 34-5 in as-joined condition without PWHT.

ID	Area (mm^2)	Max load (kN)	Max elongation (mm)	Max stress (MPa)	Max strain (%)	Yield stress (MPa)	Failure location
35-2	9.86	6.72	1.94	682	20.4	594	Within tube section outside weld
35-4	10.27	6.06	2.01	590	21.1	512	Within tube section outside weld

For a better comparison of the tensile test results between samples with and without PWHT from the same PRW process, four stress-strain curves are plotted together and shown in Figure 22. Because all four samples seen in the plot were bonded using the same joining parameters, in comparing the tensile results of samples 34-2 & 34-4 with samples 35-2 & 35-4 a comparison can be drawn between specimens tested in a PWHT condition and those tested in the 'as-joined' condition. One thing to note is all samples tested have similar yield strength and tensile strength values and all align with the values reported for the Kanthal-D material. As previously mentioned, samples 34*2 & 34-4 still showed good results where the

bond strength exceeds the yield strength of the base material. However, it can be seen here that samples joined using the PRW process, tested in the ‘as-joined’ condition produce more favorable tensile results than those tested in a PWHT condition – where the bond strength exceeds the tensile strength of the base material.

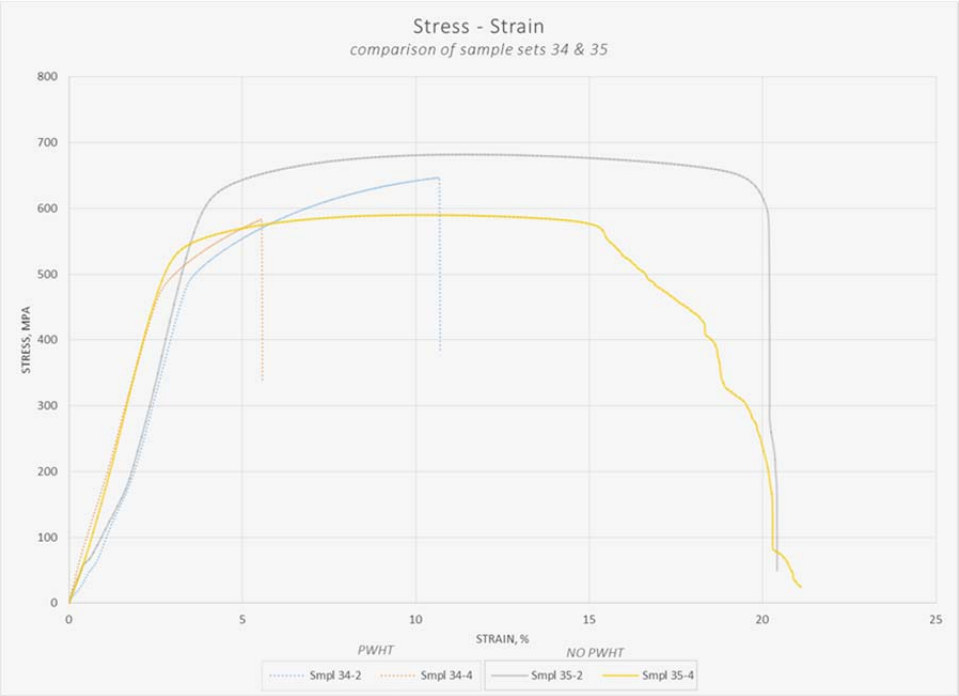

Figure 22. Comparison of tensile test results between sample set 34 (with PWHT) and set 35 (without PWHT).

Sample set 36 specimens were joined using the same joining parameters used for sample set 34 & 35. Sample set 36 specimens utilized the endplug – cladding tube weldments for hydraulic pressure burst testing. Sample set 36 specimens were subjected to a PWHT process after joining. This is for consistency with the pressure burst tested for laser welded samples which went through PWHT. The optical images of the sample set 36 after PRW joining are shown in Figure 23. The X-ray CT images of cross sectional view of the PRW bond region are shown in Figure 24 where all the bonds of sample set 36 are comparable and show equal deformation. Each bond showed good expulsion formation through the joining process. The bond line is not discernable for samples 36-1, 36-3 & 36-4 but for sample 36-2 its bond line is more visible than the other samples. All four samples were subjected to rupture testing at room temperature

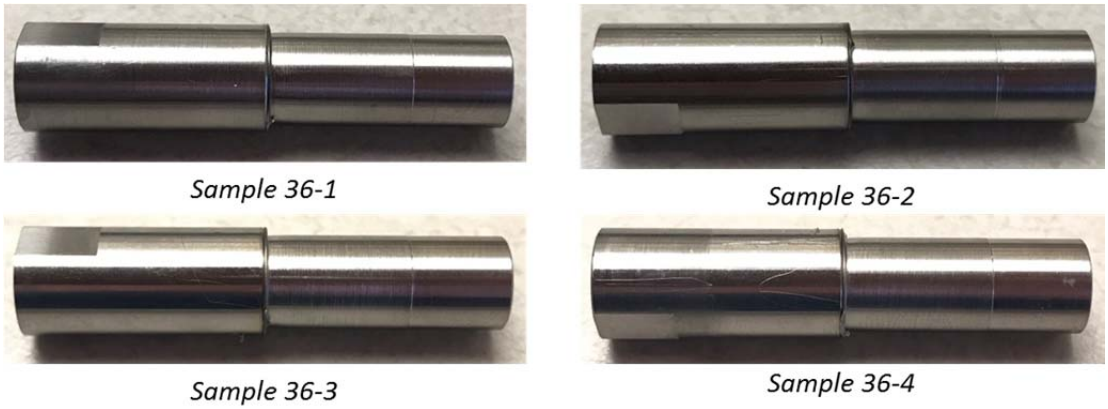

Figure 23. Images of sample Set 36 after PRW joining under the same conditions with sample set 35.

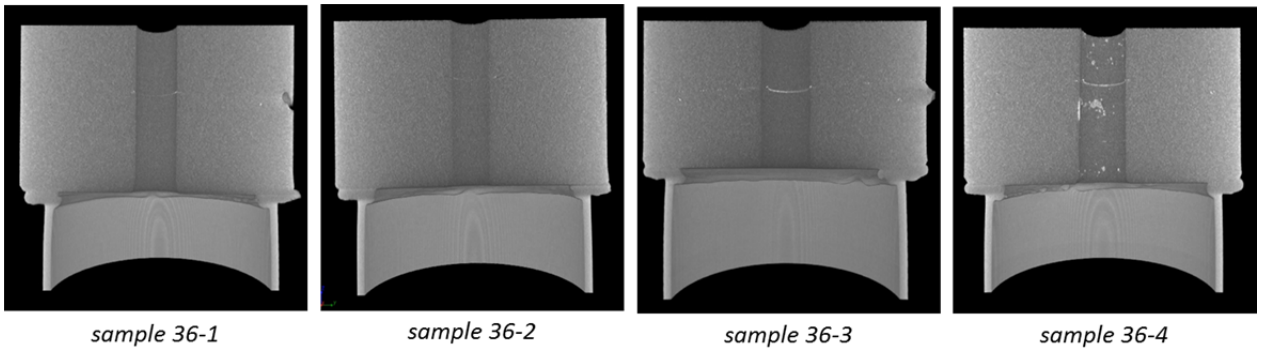

Figure 24. X-ray CT images of cross sectional view of the PRW bond region for sample set 36.

3. MICROSTRUCTURE CHARACTERIZATION OF PRW

Optical microscopy images and the EBSD grain orientation mapping of the bond region of sample 34-3 are shown in Figure 25 and Figure 26, respectively. There are no major defects seen in the bonding region that may indicate a lack of bonding between the endplug and tube weldments. Deformation and good expulsion formation are both evident. Furthermore, the disappearance of the bond line indicates the formation of a good metallurgical bond. Note that the grain texture in the weld zone is similar to that of the base material for the endplug. This is in contrast to that of laser beam weld where significantly larger grains formed in the weld zone as a result of local melting. It demonstrates the advantage of using PRW over laser beam weld for ODS alloys to minimize the disruption of the distribution of the high concentration fine oxides particles in the alloy matrix. Similar EBSD results were obtained for the sample 35-3.

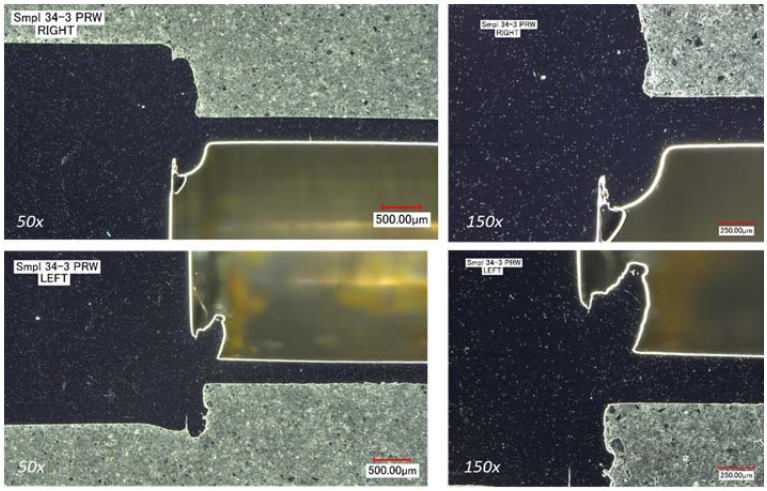

Figure 25. Optical microscopy of cross sectional view revealed the PRW bond region for sample 34-3.

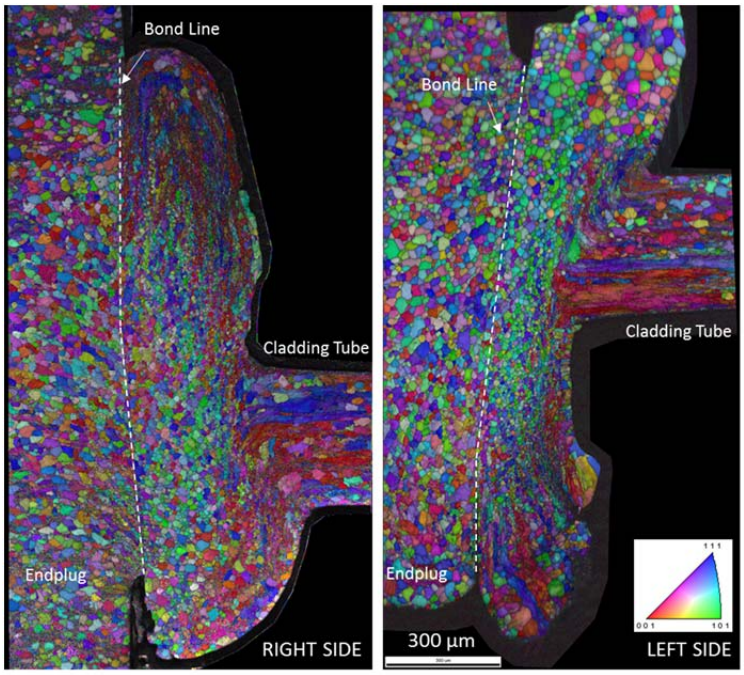

Figure 26. EBSD orientation map of the PRW bond region revealed good metallurgical bonds at the joining interface between the thin-wall cladding and endplug for sample 34-3.

An area from the RIGHT-SIDE EBSD map was selected within the tube side section of the bonding region to attempt to determine the degree of texturing observed in the grain microstructure, and to compare both cross-sections of this sample (34-3). Texture analysis shows that a large portion of the grains in the selected area are preferentially oriented between the [101] and [111] directions. The grain size within the selected region was 13.0 ± 9.1 (µm). Similarly an area from the LEFT-SIDE was selected within the tube side section of the bonding region to attempt to determine the degree of texturing observed in the grain microstructure. In this case the texture analysis shows that a large portion of the grains in the selected area are preferentially oriented towards the [101] direction. The grain size within the selected region was 16.0 ± 16.0 (µm).

4. MICROHARDNESS OF PRW BOND REGION

A grid of indents are plotted across the bonding region of samples stretching from the endplug base material to the cladding tube base material using a LECO automated micro-indentation unit with a Vickers indenter. A 100 µm spacing is used between indents in the horizontal direction and a 75 µm spacing is used between indents in the vertical direction. A loading of 100 gf and dwell time of 13 sec is used for each indent. The grid of indents extends 1.5 mm from the bond line into each section of the specimen. NOTE: the indent spacing used exceeds the minimum distance needed between the indents to avoid mechanical interference between indents. Figure 27 shows a hardness grid of the bonding region of sample 34-3 with two parallel lines showing the path of hardness contour in Figure 28. The hardness was found to fluctuate between 235 HV & 275 HV. Just from the contour plot it appears a change in hardness occurs at the bond line and there is a difference in hardness between the endplug and cladding tube. Similar results are seen in microindentation analysis for sample 35-3.

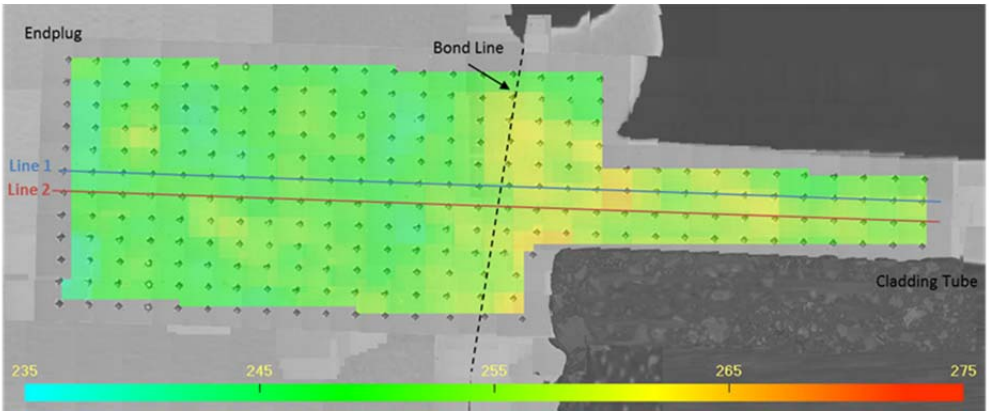

Figure 27. Optical microscopy image of microhardness indentation grid for PRW sample 34-3.

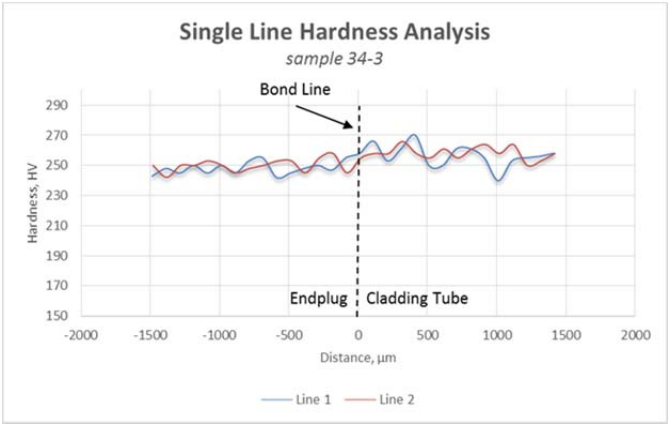

Figure 28. Hardness plot along the lines shown in the Figure 27 revealed only a minor change in the bond region.

5. HYDRAULIC PRESSURE BURST TEST OF PRW

Hydraulic pressure burst test is important to evaluate the quality of the weld. For the first HPBT test for PRW samples, the testing temperature was at approximately 25°C with a working fluid of Mineral Oil. The experimental setup for the HPBT is shown in Figure 29. The test procedure includes an initially pressurization to 1500 psi and hold for 4 min. Then the pressure was increased by 500 psi and held for 2-3 min and stepped up by a pressure increase of 500 psi until failure. In rupture testing of the PRW bonded samples the stress state of the bond is not trivial; the bond stress state is not a straight forward hoop stress state due to the proximity of the endplug and its affects from internal pressurization. It is likely the stress state of the bond is a more complex combination of a hoop and longitudinal stress states. Under internal pressurization the tube section will expand, but this expansion is not reciprocated in the endplug section, thus for all intents and purposes the bond is stressed in a manner that promotes the bond interface separating in a manner that was seen from the tested specimens.

NOTE: hoop stress was not calculated for sample set 36. As previously mentioned the bond is not placed in a hoop-ONLY stress state. For this reason the ‘thin wall approximation’ for pressure vessels could not be applied. This revelation shows the need to make some minor adjustments to the endplug design to give the bond better strength through internal pressurization. Note that for standard LWR PRW endplug attachment the cladding tube is supposed to fail before the weld under a state of internal pressure.

The HPBT results are summarized in Table 7. The images of the samples after testing are shown in Figure 30. It clearly shows that all the bursts occurred in the bond region. The pressurization profile of the HPBT is shown in Figure 31. The maximum hydraulic pressure reached (sample 36-4 at 3644 psi) before failure is much less than that seen in room temperature HPBT of the laser weld samples (sample 32-3 at 7578 psi and sample 32-4 at 7900 psi, INL/LTD-16-39760). One important finding is that the good performance in tensile test does not warrant the good performance in hydraulic pressure burst test for the PRW weldment under the same condition.

Figure 29. Images of the experimental setup for hydraulic pressure burst test at room temperature and high temperatures (left) and the details of the PRW bonded sample connected to the adapter (right).

Table 7. Hydraulic pressure burst test results for sample 36-1 through 36-4 in PWHT condition.

Sample ID	PWHT	Clad wall thickness (µm)	Mean cladding diameter (mm)	Burst pressure (psi)	Failure location
36-1	yes	340	4.62	2011	At bonding interface
36-2	yes	335	4.62	2314	At bonding interface
36-3	yes	350	4.63	2823	At bonding interface
36-4	yes	320	4.63	3644	At bonding interface

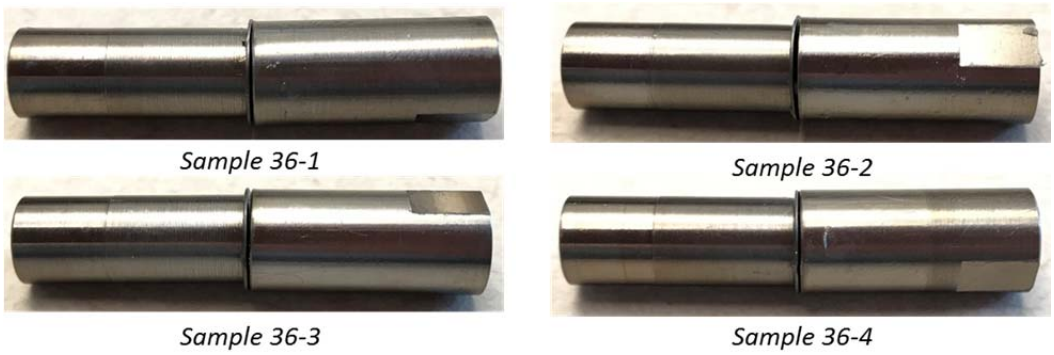

Figure 30. PRW sample 36-1 through 36-4 after pressure burst tested at room temperature in PWHT condition revealed failure at bond region.

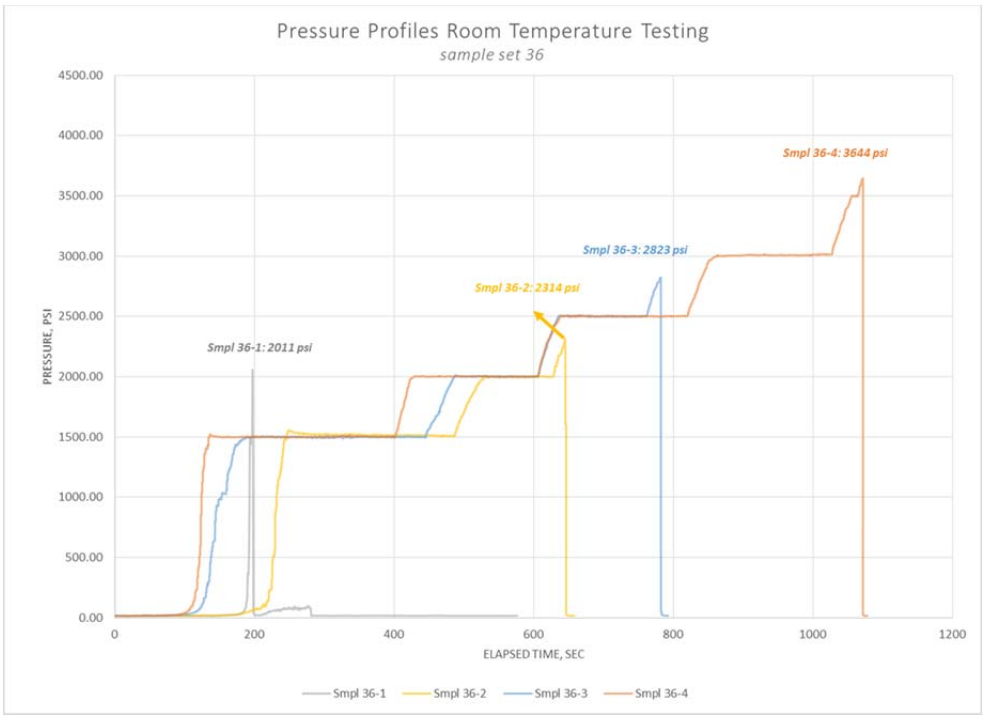

Figure 31. Pressurization profile for burst test at room temperature for sample 36-1 through 36-4.

In rupture testing of the PRW bonded samples the stress state of the bond is not trivial; the bond stress state is not a straight forward hoop stress state due to the proximity of the endplug and its effects from internal pressurization as shown in Figure 32. It is likely the stress state of the bond is a more complex combination of a hoop and longitudinal stress states. It appears that under internal pressurization the tube section will expand, but this expansion is not reciprocated in the endplug section, thus for all intents and purposes the bond is stressed in a manner that promotes the bond interface separating in a manner that was seen from the tested specimens. Further modification of the endplug is required in order to improve the mechanical strength of the PRW bond region under hydraulic pressure loading.

Figure 32. Hardness map with test grid, bond line and the lines of indents for hardness plot for PRW sample 24-5 made from Kanthal-D FeCrAl alloy.

6. CONCLUSIONS

The parametric studies for pressure resistance weld (PRW) development using a customized PRW system was carried out in the first half of FY2017. This is still in the early stage of PRW development for the project. Encouraging results were achieved as confirmed by both results of EBSD on the bond region as well as the tensile test of the PRW surrogate sample set. A reasonably good metallurgical bond was achieved at the faying interface. While the post-weld-heat-treatment improves the bond strength of the laser weld from the previous work, there seems detrimental effect of PWHT on PRW samples. Further investigation is required to identify the fundamental cause of this problem. The premature failure of PRW in hydraulic pressure burst test calls for further modification of the endplug design.